Scientific African 28 (2025) e02668

Contents lists available at ScienceDirect

Scientific African

journal homepage: www.elsevier.com/locate/sciaf

Characterization of Chitosan/ Zeolite drug delivery composite and curcumin release kinetics in a simulated pH environment

Gloria Pokuaa Manu [a,c,*], Daniel Narh [a], Bernard Asimeng [b], Nadesh Kwakye [a], Barbara Ansaah Abusuapa [a], Daniel Appuing [a], Emmanuel Nyankson [a], Johnson K. Efavi [a]

[a] Department of Materials Science and Engineering, University of Ghana, LG 77, Accra, Ghana
[b] Department of Biomedical Engineering, University of Ghana, LG 56, Accra, Ghana
[c] Department of Biochemistry, Cell and Molecular Biology, University of Ghana, Accra, Ghana

ARTICLE INFO

Editor: DR B Gyampoh

Keywords:
Curcumin
Zeolite
Chitosan
Nanocomposite
Drug delivery
Release kinetics

ABSTRACT

Cancer remains a formidable global health challenge, necessitating innovative strategies for effective drug delivery to tumor sites. This study is focused on modeling the release profile of a chitosan/zeolite nanocomposite beads delivery system encapsulating curcumin. The nanocomposites were synthesized by functionalizing zeolite with chitosan and subsequently loading curcumin. The chitosan/zeolite nanocomposite was characterized for its physicochemical properties, including surface morphology, functional groups, elemental profile, crystal structure, and drug loading capacity using SEM, FTIR, EDS, XRD, and UV–vis spectrophotometer respectively. In vitro experiments investigated the release kinetics of curcumin from the composite in simulated pH environments, providing insights into the drug release behavior. The chitosan/zeolite nanocomposite demonstrated a controlled, and sustained release of curcumin, exhibiting significant potential for optimizing therapeutic outcomes. The maximum entrapment efficiency of the chitosan/zeolite drug delivery vehicle was recorded at 84 %, indicating high efficiency in encapsulating drug molecules. Drug release kinetics were analysed using the Higuchi, Korsmeyer Peppas, Zero-Order, First-Order, and Hixson-Crowell models. The Higuchi kinetic model, which explains the release rate of drugs from an insoluble matrix based on Fickian diffusion, best explained the release of curcumin, with a correlation coefficient of $R^2 = 0.9351$. These results indicate that the zeolite functionalized chitosan nanocomposite beads hold promise as a viable platform for enhanced drug delivery, enabling prolonged drug circulation and improved therapeutic outcome.

Introduction

Cancer continues to be a global health challenge, prompting a relentless effort to devise innovative strategies for effective targeted drug delivery to the tumor sites. The progressive development of advanced drug delivery systems capable of delivering anti-cancer drugs to the tumor is paramount to enhancing the therapeutic efficacy of these agents while minimizing their systemic toxicity.

Curcumin and its derivatives have gained significant attention in the field of biomedicine and biotechnology due to its antioxidant,

* Corresponding author.
E-mail address: gpmanu@ug.edu.gh (G.P. Manu).

https://doi.org/10.1016/j.sciaf.2025.e02668
Received 31 July 2024; Received in revised form 28 February 2025; Accepted 24 March 2025
Available online 26 March 2025

anti-inflammatory, and anti-tumour abilities [1]. Multiple studies have shown curcumin's antitumor effects against prostate cancer, lung cancer, neck, and head squamous cell carcinoma, brain tumour, and breast cancer [2,3]. It is noteworthy however that curcumin has poor aqueous solubility of about 11 ng/ml [4] and degrades in alkaline conditions. It is reported that at pH< 7 curcumin degradation is much slower [5,6]. Thus, the full potential of native curcumin is limited by its low solubility, poor bioavailability, rapid metabolism, and clearance from circulation [7]. To overcome these challenges a substantial amount of dosage needs to be used hampering supplemental utilization [8,9].

The use of native curcumin has been tried in advanced biochemical methods by merging with other dietaries, hybridisation with metals, liposomal curcumin, phospholipid complexes, and conjugation with various polymeric materials and synthetic materials but these efforts have still not yielded the desired results [10,11].

To improve the medical viability of curcumin in biomedical applications novel nano-formulations of the drug is emerging as a potential means in overcoming the aforementioned therapeutic limitations for an efficient drug delivery system. Nano-formulations of curcumin into particles or encapsulation systems have been observed to greatly enhance solubility, chemical stability, and interactions with other biological entities as well as pharmacokinetic properties. The intrinsic therapeutic characteristics of native curcumin are observed to be preserved when curcumin is formed into nanoparticles leading to efficient delivery to affected tissue sites [12]. Such particle size ranges are thought to be associated with negative and positive surface charge distributions which can easily interact with cancer cells with high bioactivity between the cancer cells and drug particles due to the high available contact surface area provided by the nanoparticles [13].

Particle size plays a major role in the mode of action of drug including the interaction of particles with a biological system, tissue distribution, attachment, and rolling [14], firm adhesion of nanoparticles [15], phagocytosis [16], and accumulation [17] are all affected by the size of the particle. Due to the tailoring of a particle in a precise dimension for the purpose of getting the higher rate of absorption and permeation, it ultimately led to an incrementation in bio-distribution and longer circulation in vivo [18]. Chitosan/Zeolite nanocomposite made of nano or microporous structure, with excellent biocompatibility, and adjustable release kinetics [19] provides a versatile promising platform for delivery of potential anti-cancer agent curcumin, to cancer cells thereby serving as a novel solution to the challenges confronted by native curcumin in biomedical applications.

Zeolites are porous aluminosilicate minerals that are widely employed in adsorption, catalysis, and ion exchange applications [20]. Zeolites have a tetrahedral crystal structure formed through dense networks of AlO_4 and SiO_4 that share oxygen atoms [21–23] with a regular distribution of pores that can act as hosts for curcumin and mechanically protect its stability [24].

Zeolites are stable in water and aqueous solutions such as NaOH but disintegrate rapidly in acidic solutions [25]. Cancer cells have more acidic microenvironments than normal cells, and this distinction can be utilized to specifically detect tumour and release drugs incorporated in their pore directly to the affected areas [26].

Despite the great biomedical benefits of zeolite, they have some drawbacks. Drug molecules are mostly of smaller sizes and thus are easily released from the zeolitic structure [27]. There is also a difference in hydrophilicity between the drug molecule and the zeolite structure which reduces its loading capacity [28,29]. To improve the efficiency of the drug-carrying properties of zeolites, drug carriers need to be functionalized to overcome the differences in hydrophilicity with drugs. Surface modification of zeolite can be done through the use of functional groups such as sulfhydryl (-SH), amino (-NH2), or carboxylic (-COOH) groups, PEGylation, or other more specialized ligands including peptides, aptamers, and antibodies [30]. This modification could potentially help increase the bioavailability, specificity, cellular uptake [31,32], and efficacy of the drug delivery platform, and one promising material that meets these criteria is chitosan.

Chitosan is a linear amino polysaccharide derived from the shells of crabs, shrimps, lobsters, and other crustaceans [33]. Chitosan is a product of deacetylated chitin and consists of glucosamine, a deacetylated monomer, N-acetyl-glucosamine, an acetylated monomer, connected throughβ-,4 glycosidic bonds [34] In a chitosan structure are the presence of amino functional groups on the surface of chitosan that can interact with nanoparticles, drugs, polymers, and cells [35] and these features present great opportunities for applications medicine, food, dentistry, beverages, pharmacy, cosmetics, agriculture, and many more due to its macromolecular structure, biological activities, and its physicochemical properties [36].

Chitosan has biodegradability, biocompatibility, low toxicity, antimicrobial, and wound healing properties [37–39]. Chitosan has also demonstrated potential in cancer therapy, particularly as a dissolving agent, drug stabilizer, and controlled-release medication control, with a multipurpose platform for stimulus-responsive drug release, targeting, or image-guided medicine [40,41], and reduction of cytotoxicity to healthy cells [42].

We explore the synergistic benefits of curcumin-loaded zeolite/chitosan nanosystems to increase the bioavailability, and stability, and reduce the hydrophobicity of the zeolite platform. This study therefore aims to model the release profile of chitosan/zeolite nanocomposite beads delivery system encapsulating curcumin in a simulated environment. Rigorous characterizations of the nanocomposite's physicochemical properties, drug loading capacity, and release kinetics were observed and evaluated.

Materials and methods

3.0 Materials

Commercial chitosan, zeolite A, acetic acid, sodium hydroxide (NaOH), tetraethyl orthosilicate (TEOS), hydrochloric acid (HCL), ethanol absolute, curcumin and phosphate-buffered saline (PBS).

Synthesis of Chitosan/Zeolite nanocomposite

2 g of Chitosan was dissolved in 2 % v/v acetic acid, and zeolite nanoparticles were added with continuous stirring. Zeolite was prepared following a method described by Nyankson et al. [43]. Chitosan was functionalized with 2 % TEOS to enhance interaction with zeolite. The mixture was then allowed to react for one hour under continuous stirring at room temperature to ensure a uniform distribution of zeolite within the chitosan matrix. The nanocomposite was made into beads in an alkaline medium, washed, filtered, and dried. 25 wt. %, 50 wt. %, 75 wt. % and 100 wt. % Zeolite formulations were prepared.

Characterization of the nanocomposite

The morphology and the elemental composition of the beads were determined using a scanning electron microscopy (SEM) and Energy-dispersive X-ray spectroscopy (EDS) respectively. Drug loading capacity was determined with the UV–Vis spectroscopy (Genesys 10 s, Thermo scientific). The crystal structure of the samples was studied with the X-ray diffractometer (XRD). Functional analyses were also performed using the Fourier Transform Infrared Spectroscopy (FTIR) (Alpha ATR, Bruker).

Drug encapsulation

Curcumin (5mg/ml) was encapsulated into the 200 mg chitosan/zeolite nanocomposite beads by loading the drug into the beads under vacuum. The loaded nanocomposite beads were allowed to dry at 60 °C. The process was repeated for all the bead formulations (i.e., 25 wt. %, 50 wt. %, 75 wt. %)

Entrapment efficiency

20 mg of the loaded nanocomposite beads were placed in 10 ml of absolute ethanol, vortexed and centrifuged. UV–Visible spectrophotometry analysis was used to determine the absorbance of the supernatant at a wavelength of 430nm. The entrapment efficiency was calculated using:

$$\text{Entrapment efficiency} = ((\text{Initial drug} - \text{Free drug})/\text{Free drug}) \times 100\ \% \quad (1)$$

In vitro drug release studies

Drug release in phosphate buffered saline

20 mg of nanocomposite beads were placed in a PBS and at 2 h time intervals, samples were collected, and the released curcumin was quantified using UV–Visible spectroscopy.

pH environment simulation

A simulating pH environment of an acidic pH utilizing acidic buffers of pH 5.5, 6.0, 6.4 and 6.8 were prepared. Nanocomposite beads were introduced into this environment. The behavior of the nanocomposite, including drug release and stability, was monitored in the simulated pH environment at 2-hour time intervals. Changes in drug release profiles were recorded.

Drug release kinetics

Various kinetic models, Korsmeyer Peppas, Zero Order, First Order, Higuchi, and Hixson, were used to model the release kinetics using data from the in vitro drug release studies. The Zero-order release kinetics represent a constant release of a drug as a function of time and independent of its concentration [44]. The proportion of drug released per unit time is constant is determined with the first-order kinetic model [45]. It describes systems where the release of a drug is concentration dependent. Higuchi's mathematical model describes the dissolution and release rate of drugs from matrix systems, and it shows a plot of the amount of drug released against the square root of time [46]. Hixson Crowell's kinetic model describes the release of drugs where there are changes in the surface area and diameter of the drug delivery platforms [47,48]. Korsmeyer Peppas kinetic model is important for studying the release of drugs from polymeric systems [46].

The equation used for the zero-order kinetics is;

$$Q_t = Q_o + K_o \quad (2)$$

where Q_t is the amount of drug released at time t hours, Q_o is the initial amount of drug, and K_{ot} is the first order release constant. The equation used for the first-order kinetics is;

$$\text{Log } Q = \text{Log } Q_o - K_t / 2.303 \quad (3)$$

where K is the first order release constant. The equation used to describe the Higuchi model is;

$$-Q = K_H\sqrt{t} \quad (4)$$

where K_H is the Higuchi's release constant. The equation used to describe the Korsmeyer-Peppas; model is

$$M_t/M_\infty = kt^n \tag{5}$$

where M_t/M_∞ is the fraction of the amount of drug released at time t hours, k is the drug release constant, and n is the diffusional exponent that shows drug release mechanism. The equation used to describe the Hixson Crowell model is;

$$\sqrt[3]{W_o} = \sqrt[3]{W_i} + K_{HC}t \tag{6}$$

where W_o is the initial amount of drug, and W_i is the amount of drug at time t.

Data analysis

Statistical analysis was performed using Statistical Package for the Social Sciences (SPSS). Analysis of variance was performed to assess the differences in drug release profiles between standard PBS and the simulated pH conditions.

Results and discussion

X-ray diffraction analysis of nanocomposite beads

Fig. 1 shows the XRD pattern of pure chitosan powder and 50 wt. % zeolite. The XRD pattern of the pure chitosan powder indicates the presence of diffraction peaks of 2θ = 10.65°, and 20.16° associated with (020) and (110), respectively. The appearance of these peaks confirms the crystalline nature of chitosan in its pure form. These characteristic peaks are in agreement with the known crystallographic properties of chitosan and match precisely with the standard XRD data of chitosan (JCPDS file No 00–067–1540) [49–51]. The XRD pattern of 50 wt. % zeolite also exhibits characteristic diffraction peaks, which are indicative of the presence of zeolite. The chitosan peaks with miller indices (020) and (110) were still present in the 50 wt. % zeolite sample, but a reduction in the intensities of the diffraction peaks was observed. Notably, the diffraction peaks at 2θ = 7.18°, 30.20°, and 64.84° correspond to (200), (644), and (10,100), respectively. These peaks are known to be associated with the crystalline structure of zeolite [43]. The XRD analysis indicates that the characteristic peaks associated with both chitosan and zeolite are present in the formulations and this observation suggests that the composite materials, retain the crystalline properties of their individual components.

Fourier transform infrared spectroscopy (FTIR) spectrum of chitosan/zeolite nanocomposite beads

Fig. 2 shows FTIR spectrums of chitosan powder, 50 wt. % zeolite, and 50 wt. % curcumin-loaded chitosan/zeolite platform. Fig. 2A shows the FTIR spectrums of chitosan powder. Prominent bands in the range of 3365–3298 cm^{-1} correspond to N—H and O—H stretching vibrations [52], 2865 cm^{-1} is associated with C—H stretching [52], 1658 cm^{-1} is associated with $C = O$ stretching, Amide I and 1312 cm^{-1} associated with C—N stretching, Amide III suggests residual N-acetyl groups [53]. The appearance of bands at around 1426 and 1378 cm^{-1} confirmed the CH_2 bending and CH_3 symmetrical deformations, respectively [52], and absorption at 1026 cm^{-1} corresponds to C—O stretching [54,55] which are all characteristic of chitosan. Fig. 2B shows the FTIR spectrums of 50 wt. % zeolite. Broad bands in the range of 840–550 cm^{-1} suggest Si-O and Al-O species, characteristic of zeolite, with absorbances at 799 cm^{-1} and 666 cm^{-1} [56] and this is observed for all formulations. The absorption bands between 3750–3450 cm^{-1} correspond to OH, Si-OH, and Si-OH-Al groups [56], typical of zeolite. The peak at 666 cm^{-1} is attributed to Si-O-M species [56], where M represents the Na^+ metal

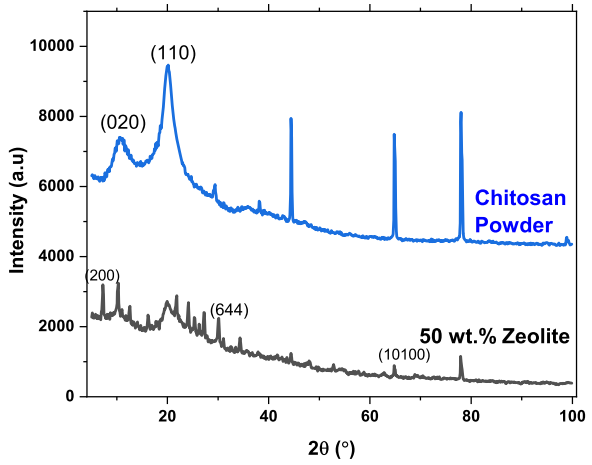

Fig. 1. XRD diffraction patterns of (A) pure chitosan powder, and (B) 50 wt. % zeolite.

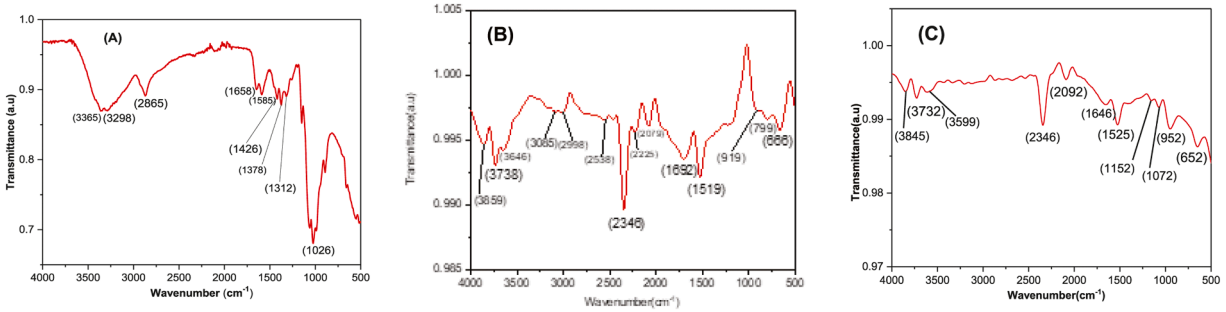

Fig. 2. FTIR spectrums of (A) chitosan powder, (B) 50 wt. % zeolite, and (C) 50 wt. % curcumin-loaded chitosan/zeolite platform.

species. Some chitosan peaks at 1692 cm^{-1} and 1519 cm^{-1} are still noticeable, with shifted values, indicating interactions or overlap with zeolite bands. Fig. 2C shows the FTIR spectrums of 50 wt. % curcumin-loaded chitosan/zeolite platform. The shifts in chitosan peaks suggest potential interactions between the two materials, providing more insights into the composite's chemical composition and interactions. The absorption band at 3599 cm^{-1} is attributed to curcumin as it is characteristic of phenolic O—H stretching [57]. Curcumin also displayed three of its signature peaks at 1646 cm^{-1} for olefinic C—H bending vibrations, 1525 cm^{-1} for $C=O$ and $C=C$ species, and 1072 cm^{-1} for C—O-C stretching vibrations [58].

Surface morphology analysis of nanocomposite

The surface morphology of the chitosan/zeolite nanocomposite was examined using SEM. Fig. 3 shows result for SEM analysis. The SEM analysis revealed a porous structure with well-dispersed zeolite nanoparticles within the chitosan matrix. Fig. 3A shows the SEM image of chitosan/zeolite nanocomposite. The result shows how the zeolite crystals have been embedded well into the chitosan structure, leading to a complete change in the morphology of the zeolite structure. Fig. 3B shows the SEM image for the functionalized nanocomposite bead, where an increase in porosity is observed after the addition of TEOS. This porosity enhancements allows for better drug encapsulation, enabling chitosan to absorb more drug molecules unto its surface and bond better with zeolite. Fig. 3C represents SEM image of curcumin loaded nanocomposite bead. The result shows that the curcumin particles have been well embedded into the chitosan/zeolite structure when compared to the SEM image of curcumin from literature [59]. [Insert Fig. 3 here]

EDS analysis for elemental profiling

The elemental composition of the chitosan/zeolite was determined using EDS. Fig. 4 shows the elemental profile of chitosan/zeolite nanocomposite of the 50 wt. % composite formulation. Table 1 shows the quantitative analysis of elements present in the sample. The carbon content in the composite ranged from approximately 29.34 % to 47.06 %, attributed to the presence of chitosan, which is rich in carbon. Oxygen content also varied between 46.03 % and 56.98 %. Oxygen is a common element in both organic (chitosan) and inorganic (zeolite) compounds. Magnesium (Mg), Aluminum (Al), Silicon (Si), Chlorine (Cl), and Calcium (Ca) are elements associated with the zeolite component of the composite. Zeolites are crystalline aluminosilicates that contain aluminum, silicon, and other elements. The presence of these elements confirms the inclusion of zeolite in chitosan.

Drug entrapment efficiency of drug vehicle

The drug loading capacity of the nanocomposite was over 80 %, indicating efficient encapsulation of curcumin (Fig. 5). After encapsulating 75 % of zeolite, entrapment efficiency gradually decreased from 84 % to 76 %. Overall, 25 and 50 wt. % zeolite showed

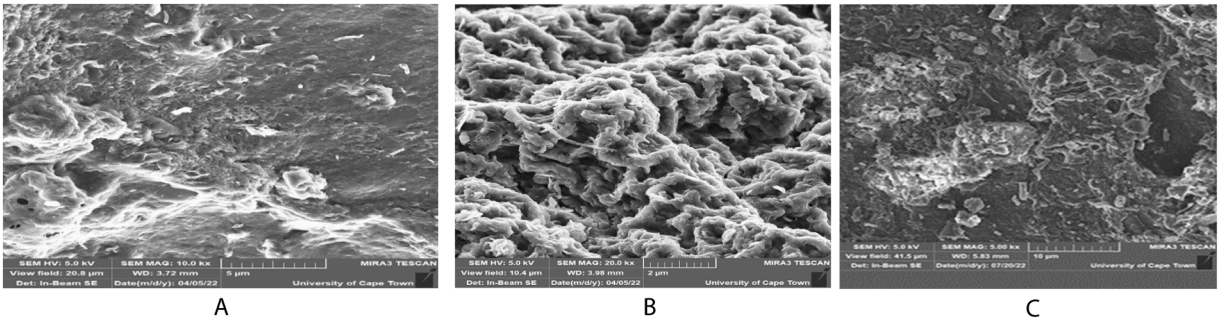

Fig. 3. SEM images of the (A) chitosan/ zeolite nanocomposite (B) Functionalized nanocomposite bead (C) curcumin loaded nanocomposite bead.

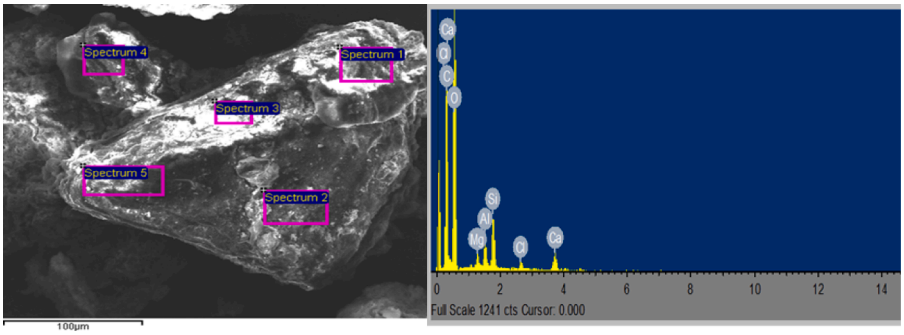

Fig. 4. Elemental profile of chitosan/zeolite nanocomposite (50 wt. % composite formulation).

Table 1
EDS analysis of synthesized chitosan/ zeolite nanocomposite.

Spectrum	C	O	Mg	Al	Si	Cl	Ca
Spectrum 1	40.06	54.95	0.76	1.17	2.14	0.41	0.51
Spectrum 2	40.55	54.32	0.59	0.99	2.09	0.37	1.1
Spectrum 3	29.34	56.98	1.25	3.64	6.41	0.32	2.05
Spectrum 4	43.19	46.03	0	0.37	0.52	1.2	8.69
Spectrum 5	47.06	51.88	0	0.19	0.5	0.18	0.19
Mean	40.04	52.83	0.52	1.27	2.33	0.5	2.51
Std. deviation	6.59	4.22	0.53	1.39	2.42	0.4	3.53

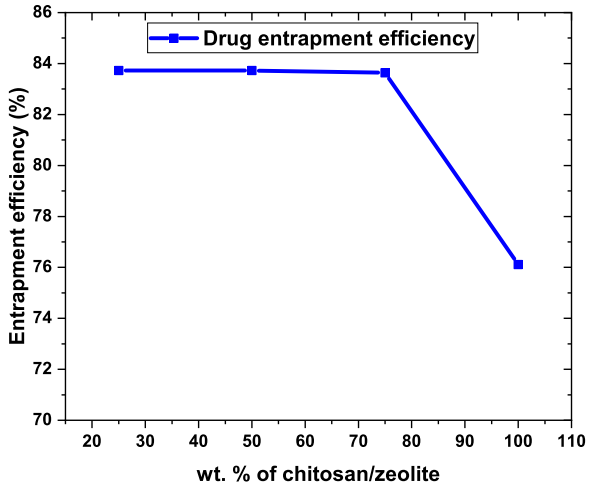

Fig. 5. Entrapment efficiency of chitosan/zeolite nanocomposite drug delivery nanocomposite for 25, 50, 75 and 100 wt. % zeolite.

the highest entrapment efficiency of 83.724 %, followed by 75 wt. % with an entrapment efficiency of 83.636 % and 100 wt. % with an entrapment efficiency of 76.109 %. The results shows that the drug delivery nanocomposite and would be very suitable for higher drug-loading capacity applications.

In vitro release profile of curcumin

The in vitro release profile of curcumin from chitosan/zeolite was evaluated in various pH conditions (5.5, 6.0, 6.4, 6.8, and 7.4) to mimic different physiological environments. This study aimed to investigate the release kinetics of curcumin to understand how different pH levels influence the drug release behavior. Fig. 6 shows the release profile of curcumin subjected to the simulated pH environment conditions. The cumulative release percentages of the drug delivery platforms were determined at specific time intervals to study the rate at which curcumin drug is been released and the stability of the platforms after the addition of chitosan.

Fig. 6A depicts the release of the standard phosphate buffered saline (PBS, pH 7.4). The release profile showed a steady release, indicative of the controlled release mechanism. All the drug delivery platforms became stabilized after 18 h. In Fig. 6B at pH = 5.5, all

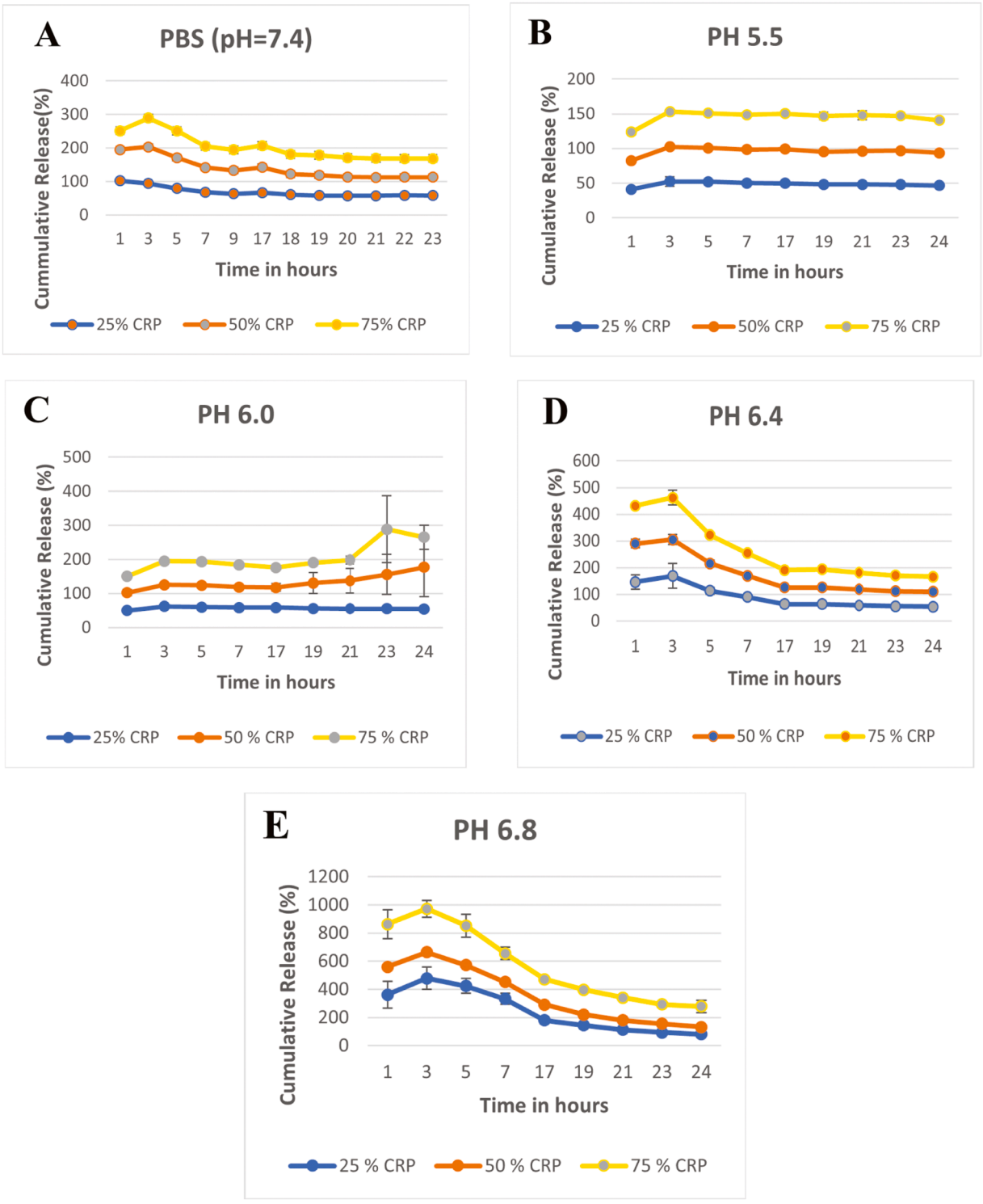

Fig. 6. Mean cumulative release values for the chitosan zeolite nanocomposite beads for 25, 50, and 75 wt. % zeolite at pH of (A) 7.4, (B) 5.5, (C) 6.0, (D) 6.4, and (E) 6.8.

drug delivery platforms displayed an initial increase in drug release followed by subsequent stabilization as depicted below. After 3 h, 50 wt. % Zeolite displayed a relatively consistent release percentage suggesting a stable release profile from the beginning. In Fig. 6C at pH = 6.0, 25 wt. % Zeolite displayed most stable drug release over an extended period of time followed by 50 and 75 wt. % Zeolite. In

Fig. 6D at pH = 6.4, all drug delivery platforms stabilized after 17 h. In Fig. 6E at pH = 6.8, 25 wt. % Zeolite recorded the highest drug release of 479.0514 % at 3 h. pH = 6.8 showed higher cumulative release compared to other simulated pH solutions.

Generally, all the drug delivery platforms showed decreasing trend in drug release over time, indicating potential stability over time. Results also showed that the nanocomposite displayed better drug release behavior compared to the standard PBS environment. Prolonged release was observed for all the different simulated pH. The initial burst release observed in the release profiles can be attributed to the rapid dissolution of curcumin on the surface of the beads, followed by a sustained release from the matrix.

Fig. 7 shows the mean cumulative release values for the chitosan zeolite nanocomposite beads. Higher mean values are observed with release mediums simulated to mimic the pH condition with the exception of pH 5.5. Analysis of variance shows a significant difference ($p = 0.001$) for drug release behavior between the simulating pH conditions and the PBS control, underscoring the influence of the simulated pH environment on drug release kinetics. Multiple comparison of the release in the different mediums using Fisher's LSD test showed a pronounced significant difference between release in PBS versus pH 6.8 ($p = 0.004$). Additionally, differences were observed among the different pH release mediums. pH 6.0 and 6.8 ($p = 0.013$), 6.4 and 5.5 ($p = 0.015$) and 6.8 and 5.5 ($p = 0.00005$) suggesting the importance of the release medium.

The results indicate that the release profile of curcumin from the chitosan/zeolite nanocomposite beads is highly dependent on the pH of the release medium and can be tailored for specific release profiles by adjusting pH. The higher rates at low pH levels are particularly relevant for targeting acidic environments, such as tumor tissues, which could enhance the therapeutic efficacy of curcumin in cancer treatment.

In vitro curcumin release kinetics

Drug release kinetics of the chitosan/zeolite composites were analysed using various kinetic models, including Higuchi, Korsmeyer Peppas, Zero-Order, First-Order, and Hixson-Crowell models. The best fit for the release data was determined by comparing the correlation coefficients (R^2) of each model.

Fig. 8 shows the release of curcumin encapsulated in chitosan/zeolite nanocomposite drug delivery platform in a simulated pH environment for A) Zero order kinetics model, B) First order kinetics model, C) Higuchi's mathematical model, D) Korsmeyer Peppas model and E) Hixson Crowell model. The models robustly described the release kinetics, with the best fit being the Higuchi model, which describe about 94 % of the release kinetics. This was followed by the Hixson-Crowell model at 78 %, the Zero Order kinetics at 64 %, the First Order kinetics at 59 %, and the Korsmeyer Peppas at 32 %. The release kinetics were best described by Higuchi's model, with a release rate constant of 20.79, followed by 2.672 for the Zero Order kinetics, 0.185 for Hixson-Crowell Model, 0.035 for the Korsmeyer-Peppas, and −0.055 for First Order kinetics. These findings highlight the predominance of a diffusion-controlled release mechanism for curcumin from the chitosan/zeolite composite, consistent with the porous structure observed in the SEM images.Fig. 9

Conclusion

The results of this study collectively emphasize the potential chitosan/zeolite nanocomposite as a drug delivery system with adaptability to the different simulated pH environmental conditions. The uniform distribution and porous structure of the composite, as demonstrated by SEM analyses, confirms a successful synthesis of the chitosan/zeolite composite delivery platform capable of encapsulating anti-cancer agents such as curcumin. Furthermore, the XRD analysis confirms the crystalline nature of pure chitosan and zeolite and the presence of characteristic diffraction peaks associated with chitosan and zeolite in all our formulations. This provides evidence that the crystalline structures of the composite materials are preserved. This preservation of crystallinity is a crucial factor to consider when assessing the structural properties and potential applications of these composite materials, especially in drug delivery systems and other biomedical applications.

The efficient drug loading capacity further underscores its suitability for encapsulating anti-cancer agents such as curcumin. The sustained release profile observed in vitro suggests its ability to provide prolonged drug exposure to cancer cells, potentially enhancing the therapeutic efficacy of curcumin. Significant difference in drug release profile for the different simulated pH conditions and PBS

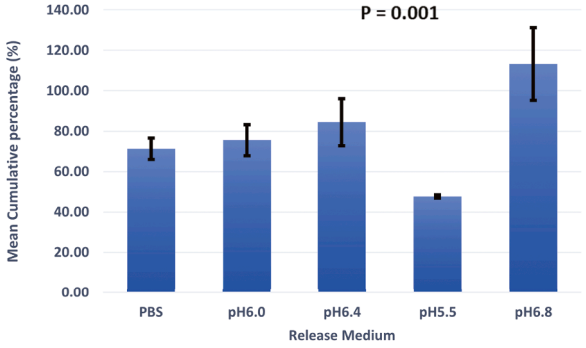

Fig. 7. Mean release profiles of 50 wt. % chitosan/ zeolite nanocomposite in the different release mediums.

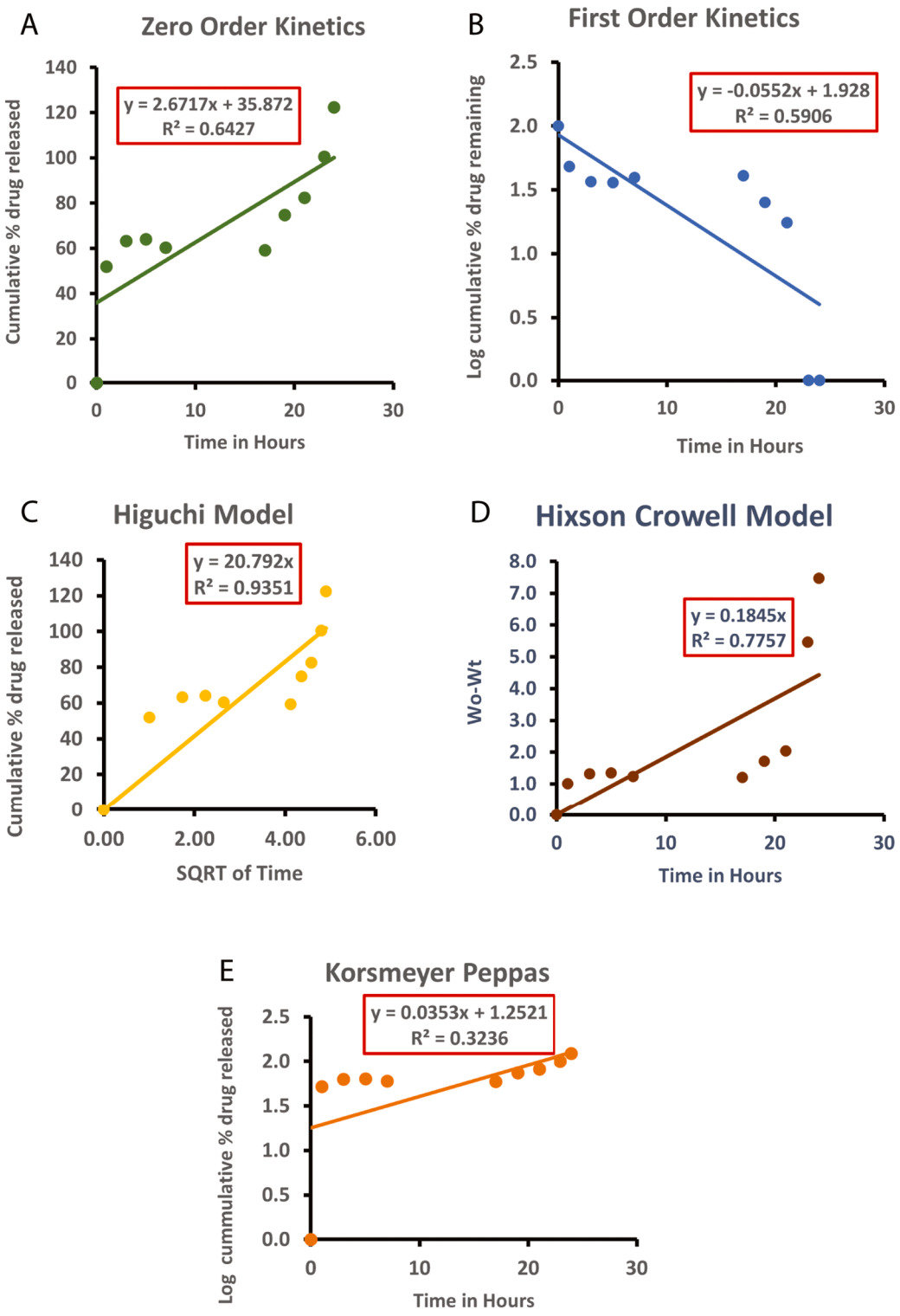

Fig. 8. Release kinetics of curcumin encapsulated in chitosan/ zeolite nanocomposite drug delivery platform in simulated pH environments using (A) Zero order kinetics model, (B) First order kinetics model, (C) Higuchi's mathematical model, (D) Korsmeyer Peppas model, and (E) Hixson Crowell model.

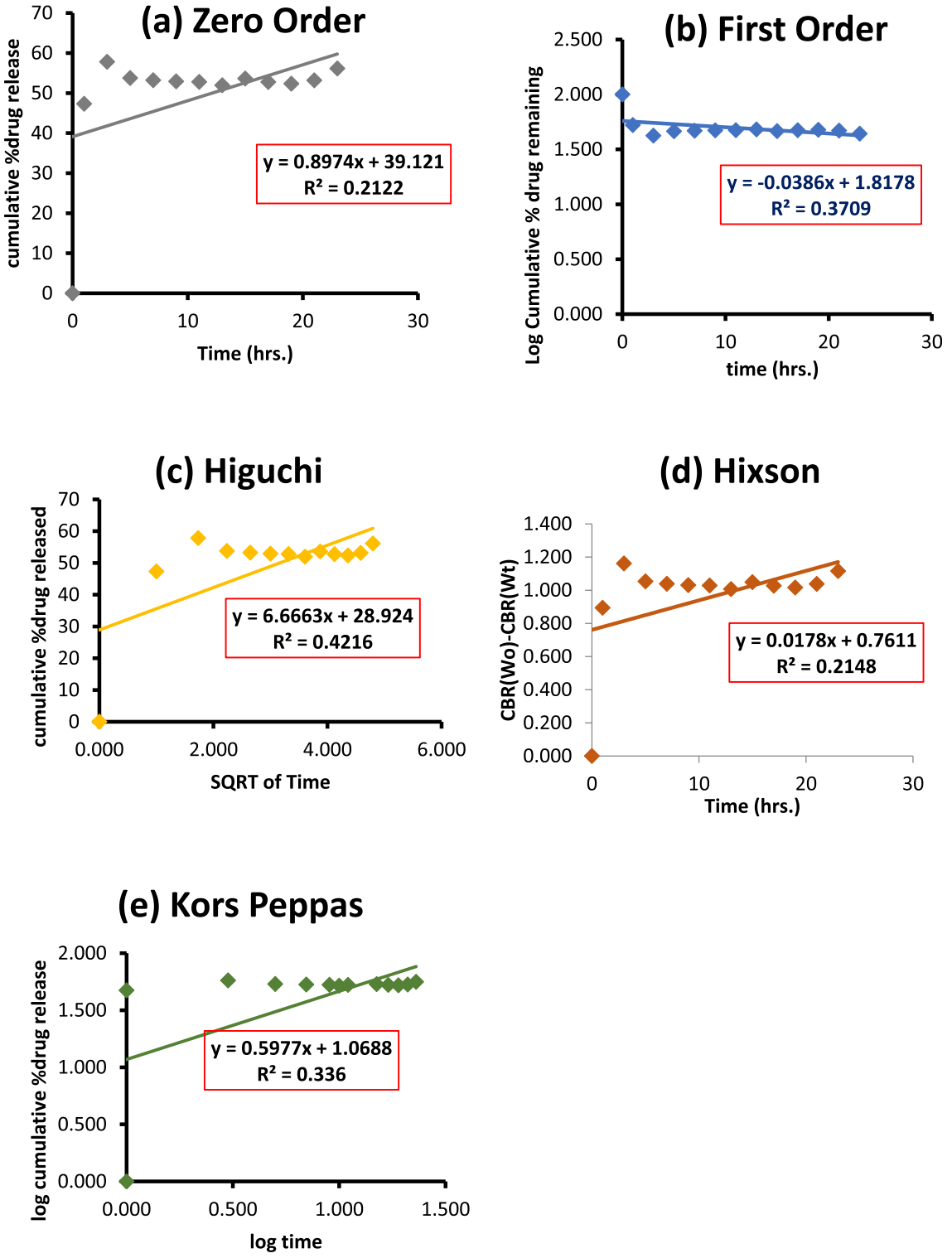

Fig. 9. Release Kinetics of chitosan/zeolite nanocomposite drug delivery platform encapsulating the anti-cancer agent curcumin in standard PBS (pH 7.4).

control highlights their influence on drug release kinetics. This finding aligns with the known variations in pH within the simulated environment, which can alter drug release from delivery platforms.

Additionally, the release kinetics model provides insights into the release mechanism, and the release rate constant highlighting the

predictability and reliability of the chitosan/zeolite nanocomposite delivery system. The biphasic release pattern, with an initial burst release followed by a gradual release, is a promising feature for achieving therapeutic drug concentrations at the tumor site while minimizing systemic exposure at the same time. The differences in the release kinetics within the different simulated release mediums indicates the necessity of considering the dynamic nature of the simulated pH environment when designing drug delivery systems and such systems should be capable of adapting to the changing conditions as well as ensuring drug availability at the tumor site.

Our findings hold significant implications for the field of cancer therapeutics and chitosan/zeolite nanocomposite could serve as a foundation for the development of tailored drug delivery systems that optimize drug release within the simulated pH environment. Future studies should focus on in vivo experiments to further validate the efficacy and safety of the drug delivery nanocomposite in animal models.

Additionally, the versatility of the nanocomposite warrants investigation into its potential for delivering various anticancer agents beyond curcumin, catering to the specific needs of different cancer types. It is important to acknowledge that, while our simulated pH environment provides valuable insights, it remains a simplified model and the complexity of the simulated pH environment in vivo involves a multitude of factors, including interactions with immune cells, stromal components, and extracellular matrix components, which may influence drug release differently.

Funding sources

This research did not receive any specific grant from funding agencies in the public, commercial, or not-for-profit sectors.

CRediT authorship contribution statement

Gloria Pokuaa Manu: Conceptualization, Investigation, Methodology, Validation, Visualization, Writing – original draft. **Daniel Narh:** Investigation, Writing – review & editing, Visualization. **Bernard Asimeng:** Resources, Supervision, Visualization, Validation. **Nadesh Kwakye:** Methodology, Investigation, Writing – original draft, Visualization. **Barbara Ansaah Abusuapa:** Methodology, Writing – review & editing, Investigation. **Daniel Appuing:** Methodology, Investigation, Writing – original draft, Visualization. **Emmanuel Nyankson:** Conceptualization, Resources, Supervision, Validation. **Johnson K. Efavi:** Conceptualization, Resources, Supervision, Writing – review & editing.

Declaration of competing interest

The authors declare that they have no known competing financial interests or personal relationships that could have appeared to influence the work reported in this paper.

Acknowledgements

We are deeply thankful to Miss Gladys Sarfowaa Kyei, a technician at the Department of Materials Science and Engineering, University of Ghana, who provided technical support throughout the course of this study. Her expertise and dedication were instrumental in ensuring the smooth operation of our experiments. We are also grateful to the national service personnel in the same department who assisted us with various tasks, including data collection and analysis.

References

[1] K. Nagahama, T. Utsumi, T. Kumano, S. Maekawa, N. Oyama, J. Kawakami, Discovery of a new function of curcumin which enhances its anticancer therapeutic potency, Sci. Rep. 6 (2016), https://doi.org/10.1038/SREP30962.
[2] K. Mansouri, S. Rasoulpoor, A. Daneshkhah, et al., Clinical effects of curcumin in enhancing cancer therapy: a systematic review, BMC Canc. 20 (2020) 791, https://doi.org/10.1186/s12885-020-07256-8.
[3] A. Giordano, G. Tommonaro, Curcumin and cancer, Nutrients 11 (2019), https://doi.org/10.3390/NU11102376.
[4] L. Zhang, W. Zhu, C. Yang, G.A. Zhai, A novel folate-modified self-microemulsifying drug delivery system of curcumin for colon targeting, Int. J. Nanomed. 7 (2012) 151, https://doi.org/10.2147/IJN.S27639.
[5] H.H. Tønnesen, J. Karlsen, Studies on curcumin and curcuminoids. VI. Kinetics of curcumin degradation in aqueous solution, Z. Leb. Unters. Forsch. 180 (1985) 402–404, https://doi.org/10.1007/BF01027775.
[6] M.J. Tuorkey, Curcumin a potent cancer preventive agent: mechanisms of cancer cell killing, Interv. Med. Appl. Sci 6 (2014) 139–146, https://doi.org/10.1556/IMAS.6.2014.4.1.
[7] B.L. Tan, M.E. Norhaizan, Curcumin combination chemotherapy: the implication and efficacy in cancer, Molecules 24 (2019) 2527, https://doi.org/10.3390/MOLECULES24142527. Page 2527 2019;24.
[8] C.D. Lao, I.V .MT. Ruffin, D. Normolle, D.D. Heath, S.I. Murray, J.M. Bailey, et al., Dose escalation of a curcuminoid formulation, BMC Compl. Altern. Med. 6 (2006), https://doi.org/10.1186/1472-6882-6-10.
[9] C. La Porte, N. Voduc, G. Zhang, I. Seguin, D. Tardiff, N. Singhal, et al., Steady-State pharmacokinetics and tolerability of trans-resveratrol 2000 mg twice daily with food, quercetin and alcohol (ethanol) in healthy human subjects, Clin. Pharmacokinet. 49 (2010) 449–454, https://doi.org/10.2165/11531820-000000000-00000.
[10] P. Anand, A.B. Kunnumakkara, R.A. Newman, B.B. Aggarwal, Bioavailability of curcumin: problems and promises, Mol. Pharm 4 (2007) 807–818, https://doi.org/10.1021/MP700113R.
[11] S. Prasad, A.K. Tyagi, B.B. Aggarwal, Recent developments in delivery, bioavailability, absorption and metabolism of curcumin: the golden pigment from golden spice, Cancer. Res. Treat. 46 (2014) 2–18, https://doi.org/10.4143/CRT.2014.46.1.2.
[12] L. Shang, K. Nienhaus, G.U. Nienhaus, Engineered nanoparticles interacting with cells: size matters, J. Nanobiotechnol. 12 (2014) 5, https://doi.org/10.1186/1477-3155-12-5.

[13] O. Afzal, A.S.A. Altamimi, M.S. Nadeem, S.I. Alzarea, W.H. Almalki, A. Tariq, et al., Nanoparticles in drug delivery: from history to therapeutic applications, Nanomaterials 12 (2022), https://doi.org/10.3390/NANO12244494.
[14] K.W. Powers, M. Palazuelos, B.M. Moudgil, S.M. Roberts, Characterization of the size, shape, and state of dispersion of nanoparticles for toxicological studies, Nanotoxicology 1 (2007) 42–51, https://doi.org/10.1080/17435390701314902.
[15] V.R. Shinde Patil, C.J. Campbell, Y.H. Yun, S.M. Slack, D.J Goetz, Particle diameter influences adhesion under flow, Biophys. J. 80 (2001) 1733–1743, https://doi.org/10.1016/S0006-3495(01)76144-9.
[16] J.A. Champion, A. Walker, S. Mitragotri, Role of particle size in phagocytosis of polymeric microspheres, Pharm. Res. 25 (2008) 1815–1821, https://doi.org/10.1007/S11095-008-9562-Y.
[17] S.E.A. Gratton, P.A. Ropp, P.D. Pohlhaus, J.C. Luft, V.J. Madden, M.E. Napier, et al., The effect of particle design on cellular internalization pathways, Proc. Natl. Acad. Sci. U. S. A 105 (2008) 11613–11618, https://doi.org/10.1073/PNAS.0801763105.
[18] M. Gera, N. Sharma, M. Ghosh, D.L. Huynh, S.J. Lee, T. Min, et al., Nanoformulations of curcumin: an emerging paradigm for improved remedial application, Oncotarget 8 (2017) 66680–66698, https://doi.org/10.18632/ONCOTARGET.19164.
[19] H. Derakhshankhah, S. Jafari, S. Sarvari, E. Barzegari, F. Moakedi, M. Ghorbani, et al., Biomedical applications of zeolitic nanoparticles, with an emphasis on medical interventions, Int. J. Nanomed. 15 (2020) 363, https://doi.org/10.2147/IJN.S234573.
[20] E. Pérez-Botella, S. Valencia, F. Rey, Zeolites in adsorption processes: state of the art and future prospects, Chem. Rev 122 (2022) 17647, https://doi.org/10.1021/ACS.CHEMREV.2C00140.
[21] S.K. Pavelić, J.S. Medica, D. Gumbarević, A. Filošević, N. Pržulj, K. Pavelić, Critical review on Zeolite clinoptilolite safety and medical applications in vivo, Front. Pharmacol. 9 (2018), https://doi.org/10.3389/FPHAR.2018.01350.
[22] A. Mastinu, A. Kumar, G. Maccarinelli, S.A. Bonini, M. Premoli, F. Aria, et al., Zeolite clinoptilolite: therapeutic virtues of an ancient mineral, Molecules 24 (2019), https://doi.org/10.3390/MOLECULES24081517.
[23] Jha B., Singh D. Fly ash zeolites: innovations, applications, and directions. 2016.
[24] C. Karavasili, L. Kokove, I. Kontopoulou, G.K. Eleftheriadis, N. Bouropoulos, D.G. Fatouros, Dissolution enhancement of the poorly soluble drug nifedipine by co-spray drying with microporous zeolite beta, J. Drug. Deliv. Sci. Technol 35 (2016) 91–97, https://doi.org/10.1016/J.JDDST.2016.06.004.
[25] J. Hao, I.S. Milašin, Z.B. Eken, M. Mravak-Stipetic, K. Pavelić, F. Ozer, Effects of Zeolite as a drug delivery system on cancer therapy: a systematic review, Molecules 26 (2021), https://doi.org/10.3390/MOLECULES26206196.
[26] Z. Lei, Q. Tang, Y. Ju, Y. Lin, X. Bai, H. Luo, et al., Block copolymer@ZIF-8 nanocomposites as a pH-responsive multi-steps release system for controlled drug delivery, J. Biomater. Sci. Polym. Ed 31 (2020) 695–711, https://doi.org/10.1080/09205063.2020.1713451.
[27] M. Servatan, P. Zarrintaj, G. Mahmodi, S.J. Kim, M.R. Ganjali, M.R. Saeb, et al., Zeolites in drug delivery: progress, challenges and opportunities, Drug. Discov. Today 25 (2020) 642–656, https://doi.org/10.1016/J.DRUDIS.2020.02.005.
[28] C. Serri, B. de Gennaro, V. Quagliariello, R.V. Iaffaioli, G. De Rosa, L. Catalanotti, et al., Surface modified zeolite-based granulates for the sustained release of diclofenac sodium, Eur. J. Pharm. Sci. 99 (2017) 202–208, https://doi.org/10.1016/J.EJPS.2016.12.019.
[29] M.M. Salim, N.A.N.N. Malek, Characterization and antibacterial activity of silver exchanged regenerated NaY zeolite from surfactant-modified NaY zeolite, Mater. Sci. Eng. C. Mater. Biol. Appl 59 (2016) 70–77, https://doi.org/10.1016/J.MSEC.2015.09.099.
[30] N. Vilaça, A.R. Bertão, E.A. Prasetyanto, S. Granja, M. Costa, R. Fernandes, et al., Surface functionalization of zeolite-based drug delivery systems enhances their antitumoral activity in vivo, Mater. Sci. Eng. C. Mater. Biol. Appl 120 (2021) 111721, https://doi.org/10.1016/J.MSEC.2020.111721.
[31] R. Mout, D.F. Moyano, S. Rana, V.M. Rotello, Surface functionalization of nanoparticles for nanomedicine, Chem. Soc. Rev 41 (2012) 2539–2544, https://doi.org/10.1039/C2CS15294K.
[32] C. Seca, A. Ferraresi, S. Phadngam, C. Vidoni, C. Isidoro, Autophagy-dependent toxicity of amino-functionalized nanoparticles in ovarian cancer cells, J. Mater. Chem. B 7 (2019) 5376–5391, https://doi.org/10.1039/C9TB00935C.
[33] P.N. Dave, A. Gor, Natural polysaccharide-based hydrogels and nanomaterials: recent trends and their applications, Handb. Nanomater. Ind. Appl. (2018) 36–66, https://doi.org/10.1016/B978-0-12-813351-4.00003-1.
[34] V.M. Gaspar, A.F. Moreira, D. de Melo-Diogo, E.C. Costa, J.A. Queiroz, F. Sousa, et al., Multifunctional nanocarriers for codelivery of nucleic acids and chemotherapeutics to cancer cells, Nanobiomater. Med. Imaging (2016) 163–207, https://doi.org/10.1016/B978-0-323-41736-5.00006-6.
[35] M. Nurunnabi, V. Revuri, K.M. Huh, Lee Y kyu, Polysaccharide based nano/microformulation: an effective and versatile oral drug delivery system, Nanostruc. Oral. Med. (2017) 409–433, https://doi.org/10.1016/B978-0-323-47720-8.00015-8.
[36] N. Morin-Crini, E. Lichtfouse, G. Torri, G. Crini, Applications of chitosan in food, pharmaceuticals, medicine, cosmetics, agriculture, textiles, pulp and paper, biotechnology, and environmental chemistry, Environ. Chem. Lett. 2019. 17 4 (2019) 1667–1692, https://doi.org/10.1007/S10311-019-00904-X, 17.
[37] R. Singh, K. Shitiz, A. Singh, Chitin and chitosan: biopolymers for wound management, Int. Wound. J 14 (2017) 1276, https://doi.org/10.1111/IWJ.12797.
[38] M.G. Peter, Applications and environmental aspects of Chitin and Chitosan, J. Macromol. Sci. 32 (2006) 629–640, https://doi.org/10.1080/10601329508010276.
[39] R.N. Tharanathan, F.S. Kittur, Chitin-the undisputed biomolecule of great potential, Crit. Rev. Food Sci. Nutr 43 (2003) 61–87, https://doi.org/10.1080/10408690390826455.
[40] Y. Herdiana, N. Wathoni, D. Gozali, S. Shamsuddin, M. Muchtaridi, Chitosan-based Nano-smart drug delivery system in breast cancer therapy, Pharmaceutics 15 (2023) 879, https://doi.org/10.3390/pharmaceutics15030879.
[41] C.M.J. Hu, S. Aryal, L. Zhang, Nanoparticle-assisted combination therapies for effective cancer treatment, Ther. Deliv 1 (2010) 323–334, https://doi.org/10.4155/TDE.10.13.
[42] A.A. Alexander-Bryant, W.S. Vanden Berg-Foels, X. Wen, Bioengineering strategies for designing targeted cancer therapies, Adv. Cancer. Res 118 (2013) 1–59, https://doi.org/10.1016/B978-0-12-407173-5.00002-9.
[43] E. Nyankson, J.K. Efavi, A. Yaya, G. Manu, K. Asare, J. Daafuor, et al., Synthesis and characterisation of zeolite-A and Zn-exchanged zeolite-A based on natural aluminosilicates and their potential applications, Cogent. Eng 5 (2018), https://doi.org/10.1080/23311916.2018.1440480.
[44] A. Gokhale, Achieving zero-order release kinetics using multi-step diffusion-based drug delivery, Pharm. Technol. Eur. 26 (2014) 38–42. https://www.pharmtech.com/view/achieving-zero-order-release-kinetics-using-multi-step-diffusion-based-drug-delivery (accessed July 15, 2023).
[45] A. Lisik, W. Musiał, Conductomeric evaluation of the release kinetics of active substances from pharmaceutical preparations containing iron ions, Mater. (Basel) 12 (2019) 730, https://doi.org/10.3390/MA12050730.
[46] M.L. Bruschi, Mathematical models of drug release, Strateg. Modify Drug Release Pharm. Syst. (2015) 63–86, https://doi.org/10.1016/B978-0-08-100092-2.00005-9.
[47] I. Mohamed Rizwan, N. Damodharan, Mathematical modelling of dissolution kinetics in dosage forms, Res. J. Pharm. Technol 13 (2020) 1339–1345, https://doi.org/10.5958/0974-360X.2020.00247.4.
[48] Understanding release kinetics of biopolymer drug delivery microcapsules for biomedical applications, Mater. Sci. Eng. 168 (2010) 127–131, https://doi.org/10.1016/j.mseb.2009.11.006.
[49] J. Kumirska, M. Czerwicka, Z. Kaczyński, A. Bychowska, K. Brzozowski, J. Thöming, et al., Application of spectroscopic methods for structural analysis of Chitin and Chitosan, Mar. Drugs 8 (2010) 1567–1636, https://doi.org/10.3390/MD8051567.
[50] R. Saud, S. Pokhrel, P.N. Yadav, Synthesis, characterization and antimicrobial activity of maltol functionalized chitosan derivatives, J. Macromol. Sci. 56 (2019) 375–383, https://doi.org/10.1080/10601325.2019.1578616.
[51] M. Hajjaji, A. Alagui, N. Joly, P. Martin, β-chitosan-clay films: characterization and antibacterial study using response surface methodology, Polym. Renew. Resour. 13 (2022) 223–242, https://doi.org/10.1177/20412479221128967.
[52] M.F. Queiroz, K.R.T. Melo, D.A. Sabry, G.L. Sassaki, H.A.O. Rocha, Does the use of Chitosan contribute to oxalate kidney stone formation? Mar. Drugs 13 (2014) 141–158, https://doi.org/10.3390/md13010141.

[53] S.H. Lim, S.M. Hudson, Synthesis and antimicrobial activity of a water-soluble chitosan derivative with a fiber-reactive group, Carbohydr. Res 339 (2004) 313–319, https://doi.org/10.1016/j.carres.2003.10.024.
[54] Pati S., Chatterji A., Dash B.P., Raveen Nelson B., Sarkar T., Shahimi S. Structural characterization and antioxidant potential of Chitosan byγ-irradiation from the carapace of horseshoe crab polymers (Basel) 2020; 12:2361. doi: 10.3390/polym12102361.
[55] C. Song, H. Yu, M. Zhang, Y. Yang, G. Zhang, Physicochemical properties and antioxidant activity of chitosan from the blowfly Chrysomya megacephala larvae, Int. J. Biol. Macromol 60 (2013) 347–354, https://doi.org/10.1016/J.IJBIOMAC.2013.05.039.
[56] D. Nibou, S. Amokrane, H. Mekatel, N. Lebaili, Elaboration and characterization of solid materials of types zeolite NaA and faujasite NaY exchanged by zinc metallic ions Zn^{2+}, Phys. Procedia 2 (2009) 1433–1440, https://doi.org/10.1016/J.PHPRO.2009.11.113.
[57] M.M. Yallapu, M. Jaggi, S.C. Chauhan, Poly(β-cyclodextrin)/curcumin self-assembly: a novel approach to improve curcumin delivery and its therapeutic efficacy in prostate cancer cells, Macromol. Biosci 10 (2010) 1141–1151, https://doi.org/10.1002/MABI.201000084.
[58] M.M. Yallapu, M. Jaggi, S.C. Chauhan, β-cyclodextrin-curcumin self-assembly enhances curcumin delivery in prostate cancer cells, Colloids. Surf. B. Biointerfaces 79 (2010) 113–125, https://doi.org/10.1016/J.COLSURFB.2010.03.039.
[59] I. Mohamed Rizwan, N. Damodharan, Mathematical modelling of dissolution kinetics in dosage forms, Res. J. Pharm. Technol 13 (2020) 1339–1345, https://doi.org/10.5958/0974-360X.2020.00247.4.